ACS APPLIED MATERIALS & INTERFACES

Research Article

www.acsami.org

Properties and Application Perspective of Hybrid Titania-Silica Patterns Fabricated by Inkjet Printing

Petr Dzik,*[,†] Michal Veselý,[†] Marko Kete,[‡] Egon Pavlica,[‡] Urška Lavrenčič Štangar,[‡] and Michael Neumann-Spallart[§]

[†]Faculty of Chemistry, Brno University of Technology, Purkynova 118, 612 00 Brno, Czech Republic

[‡]School of Environmental Sciences, University of Nova Gorica, Vipavska 13, SI-5000 Rožna dolina, Nova Gorica Slovenia

[§]Groupe d'Étude de la Matière Condensée (GEMaC), CNRS/Université de Versailles, 45, avenue des États-Unis, 78035 Versailles CEDEX, France

ABSTRACT: A hybrid titania-silica cold-setting sol has been developed that can be deposited onto a wide variety of surfaces without the need for high-temperature fixing and that is suitable for material printing deposition. Thin hybrid titania-silica coatings were patterned onto glass and PET substrates by inkjet printing. Well-defined hybrid titania-silica patterns, with thicknesses ranging from 40 to 400 nm, were fabricated by overprinting 1 to 10 layers. Excellent mechanical, optical, and photocatalytic properties were observed, making the reported material well suited for the fabrication of transparent self-cleaning coatings both on mineral and organic substrates. The printed patterns exhibit photoelectrochemical activity that can be further improved by thermal or photonic curing. A concept of fully printed interdigitated photoelectrochemical cells on flexible PET substrates utilizing the reported hybrid photocatalyst is disclosed as well.

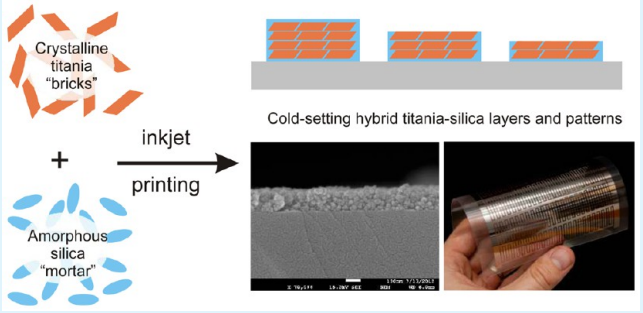

KEYWORDS: *photocatalysis, material printing, inkjet printing, direct patterning, titanium dioxide, silica, binder*

1. INTRODUCTION

Metal oxide semiconductors, especially titanium dioxide, and their related photocatalytic processes have been the subjects of intensive research for the past four decades. The primary discovery of the photoelectrochemical splitting of water on titanium dioxide electrodes[1] has gradually evolved into a broad technological field of applied photocatalysis. This technology may have the potential to address some of the most urgent technological challenges,[2] especially if solar light is employed as the irradiation source.[3]

Basically, any photocatalytic process is initiated by the photogeneration of electron−hole pairs in a semiconductor crystal lattice, which results from the absorption of UV (or even visible light in the case of a narrow band gap semiconductor) quanta of energy equal to or higher than the corresponding band gap. The electrons and holes can either recombine, dissipating the absorbed energy as heat, or remain separated and available for redox reactions with electron-donor or acceptor species adsorbed at the semiconductor surface or localized in the electrical double layer surrounding the particle.[4]

While photocatalytic processes utilizing the slurried form of a catalyst deliver excellent performances because of their inherently high surface area, a photocatalyst immobilized onto a suitable support is usually the preferred form for practical applications. Upon immobilization, the free surface of the catalyst inevitably decreases, resulting into a loss of catalytic performance because of limited mass transport. Conversely, immobilized systems are not burdened by the need for catalyst recovery, which could otherwise prohibitively increase the operational costs. Both the gas phase deposition and the wet coating method have been successfully adopted for the preparation of immobilized photocatalyst layers.[5]

Titanium dioxide is definitely the most popular and promising material among transition metal semiconductors for photocatalytic applications. TiO_2 is both widely commercially available and also easy to prepare by various methods that yield different titania grades. It has been successfully used for the design of many commercial devices that decompose hazardous substances in our living environment based on the strong oxidizing power of its photogenerated holes and its high photostability. So far, we have witnessed the proposal and successful application of photocatalytic phenomena for water purification[6] and disinfection,[7] toxic waste treatment,[8] air purification and deodorizing,[9] and self-cleaning,[10] self-disinfecting,[11] and superhydrophilic antifogging[12] surfaces.

Self-cleaning surfaces generally belong to one of two types of surfaces: hydrophobic or hydrophilic. The main characteristic of hydrophobic surfaces containing specific polymers or waxes is a

Received: October 16, 2014
Accepted: July 7, 2015
Published: July 7, 2015

DOI: 10.1021/acsami.5b03494
ACS Appl. Mater. Interfaces 2015, 7, 16177−16190

very high contact angle between the water droplet and the support (>150°). Consequently, the adhesion of the dirty spherical water droplet to the support is prevented. Another possible approach to prevent the adhesion of water droplets is the use of hydrophilic coatings composed of transition metal oxides, most typically TiO_2, as explained above. Such coatings contribute to self-cleaning for two reasons. First, the presence of UV radiation and water molecules induce chemical changes on the surfaces (oxygen vacancies are created and subsequently filled by hydroxyl ions), causing them to become highly hydrophilic with a very low water contact angle (<5°). Such high hydrophilicity enhances the adhesion of water, and the slightly adsorbed inorganic dirt particles are easily washed away by e.g., rainwater. Second, organic debris deposits are photocatalytically destroyed by the photogenerated hole−electron pairs.

Although titania coatings have been fabricated by countless different processes, wet coating techniques constitute a very popular and usually simpler alternative to vacuum processes requiring sophisticated instrumentation. Many different wet coating techniques have been proposed, such as dip-, spin-, or spray-coating, doctor blade, or roller spreading.[13] However, these traditional methods have been recently replaced by modified printing techniques,[14] among which inkjet material deposition seems to be especially promising. The technique shares the basic principles of conventional inkjet printing,[15] i.e., tiny droplets of a low-viscosity liquid are precisely deposited onto a substrate by means of a thermal or a piezoelectric printhead.[16] In the case of material printing, the ink is a specially formulated liquid used for transporting a functional component onto the substrate surface.[17]

However, to perform any of the above-mentioned traditional wet coating processes or novel modified printing techniques, a suitable liquid formulation carrying the functional component (titanium dioxide photocatalyst in this case) needs to be developed. Two distinct approaches to this task can be easily identified:

The first approach is based on the sol−gel process, i.e., soluble titanium salts and/or titanium alkoxides are complexed by suitable chelates, precross-linked by partial hydrolysis, and the resulting metastable colloidal sols are then coated onto a substrate, gelled, and converted into dense or porous oxide layers.[18] Thermal calcination is the most common way to achieve this conversion, but low temperature alternatives are available.[19] Inkjettable titania formulations based on this approach were reported by Arin[20] and Manga.[21] The authors of the present paper have reported the deposition of conventional sol−gel formulations based on tetraisopropoxy titanate and acetyl acetone by a modified office inkjet printer.[22] Thick multilayer coatings were printed with the help of poly(ethylene glycol) acting as a viscosity-modifying, templating, and anticracking agent.[23] Sols based on reverse micelle templates[24] were also successfully adapted for inkjet printing, and the printed patterns showed interesting sensing properties as well as photocatalytic activity.[25]

Much experimental attention has also been paid to explore the second possible approach leading to printed TiO_2 films. This alternative route is based on the synthesis of stable colloidal suspensions of nanocrystalline TiO_2 followed by the delivery of this suspension onto a substrate by means of inkjet printing. Bernacka-Wojcik and co-workers recently demonstrated[26] a disposable biosensor integrating an inkjet printed photodetector fabricated by printing a commercial dispersion of titania particles with a desktop office printer equipped with a thermal inkjet head. A similar approach was adopted by Yang et al.[27] who used a dispersion of TiO_2 printed by a modified office inkjet printer to produce an oxygen demand sensing photoanode and by Arin et al.[28] who fabricated photocatalytically active TiO_2 films by inkjet printing of nanoparticle suspensions obtained from microwave-assisted hydrothermal synthesis. The authors of the present paper have recently reported the fabrication of titania patterns by inkjet printing of rutile nanodispersions originating from hydrothermal processes.[29]

The obvious issue inherently associated with this second approach is the adhesion of the deposited material to the substrate. The aggregated nanoparticles left after solvent evaporation only have very limited adhesion to the substrate and need to be fixed in some way. The above-referenced examples employed the most common solution to this problem, i.e., heat treatment at 300−500 °C. However, more sophisticated solutions have been reported. Cold-setting processes yielding stable titania layers are very attractive for the fabrication of photoelectrochemical functional or auxiliary coatings on the surface of heat-sensitive substrates. This is especially true in the case of dye-sensitized solar cells, where the adoption of cheap flexible polymer supports is considered a necessary condition for commercial success. A great deal of attention has therefore been paid to this problem, and several interesting processes have been reported so far. The key lies in the mechanisms of titania layer building, and the processes to address the above-mentioned necessary condition included e.g., UV-curing of a titanium alkoxide binder,[30] incorporation of a mineral binder such as amorphous silica,[31] atomic layer deposition over a mesoporous template,[32] low temperature CVD fed a with custom molecular precursor,[33] titanium alkoxide decomposition in supercritical carbon dioxide,[34] or cold isostatic pressing of standard P-25 grade titania.[35]

In this paper, we communicate our development of a hybrid titania-silica cold-setting sol that can be deposited onto a wide variety of surfaces without the need for high-temperature fixing and that is suitable for material printing. We employed a low-temperature modification of the so-called brick-and-mortar strategy[36] based on mixing prefabricated nanocrystalline titania "bricks" with "mortar" consisting of an amorphous silica binder.

The synthetic route of the "bricks", i.e., the photocatalytically active component, was inspired by Yun et al.[37] who prepared a sol starting from titanium tetraisopropoxide in acidic aqueous solution and kept it for several hours under reflux to induce the crystallization of the amorphous TiO_2 already present in the primary reaction mixture. The "mortar" consisting of amorphous SiO_2 is capable of enhancing both the mechanical and physicochemical properties of the coatings. Apart from acting as the binding agent,[31] colloidal silica can improve adhesion,[38] increase the natural hydrophilicity of the material,[39] promote the adsorption of reactants,[40] and influence the thermal stability.[41]

The original titania-silica stock dispersion[42] was further modified by the addition of a suitable solvent system, and thus, a stable inkjettable formulation was developed. Thin hybrid titania-silica coatings were patterned onto glass and PET substrates by inkjet printing, and their material characteristics were closely investigated. A detailed report of the material properties of the resulting coatings, a brief evidence of their photocatalytic activity, and an envisaged proof of concept application are disclosed in this paper.

2. EXPERIMENTAL SECTION

2.1. Chemicals and Substrates. The chemicals in this study were used as purchased: terephthalic acid (TPA) from Alfa Aesar, NaOH

DOI: 10.1021/acsami.5b03494
ACS Appl. Mater. Interfaces 2015, 7, 16177−16190

from Sigma-Aldrich, titanium(IV) tetraisopropoxide (TTIP) and hydroxyethyl-cellulose (HEC) from Fluka (Product Nr.: 54290), tetraethoxysilane from J.T. Baker, acetonitrile from Fischer Scientific, 96% ethanol from Itrij, Levasil 200/30% colloidal SiO_2 from H.C. Starck, propane-2-ol and ethylene glycol from Penta, and propoxyethanol from Sigma-Aldrich. All aqueous solutions were prepared by using highly pure water from the NANOpure system (Barnstead).

Soda-lime glass plates were used as substrates (microscope slides 26 mm × 76 mm, Paul Marienfeld, Germany and custom cut 50 × 50 mm, Merci, Czech Republic). Commercial 2 mm-thick FTO-coated glass (Sigma-Aldrich) cut in 25 × 45 mm slides was used for the fabrication of samples for photoelectrochemical analysis. These slides were scratched parallel to the longer edge with a diamond knife, and two isolated FTO strips were thus created on a single substrate. Substrates of both types were sonicated in Neodisher LM alkaline detergent, rinsed with isopropyl alcohol, and dried in a flow of nitrogen.

2.2. Sol Synthesis. The preparation procedure of the titania/silica sol is described in detail in the patent application.[42] Herein, a short description is given: in a round-bottom flask, absolute ethanol (6.78 mL) was mixed with TTIP (41.67 mL). Separately, 2.778 mL of perchloric acid (70%) was added to 250 mL of double deionized water. This acidified water was then added dropwise to the mixture of absolute ethanol and TTIP under stirring. Then, the reflux was started, and after 48 h, a stable sol, denoted sol A, was obtained. Separately, TEOS (1.11 mL) and Levasil 200/30% (1.7 mL) were mixed in a beaker, HCl (32%, 30 μL) was added under stirring, and finally, 1-propanol (5 mL) was added to produce the silica binder solution. The final sol used in this study was prepared by mixing sol A with the SiO_2 binder. The molar ratio of TiO_2 and SiO_2 was set to 1:1 according to the results of previous testing. This particular ratio was denoted 1A, and the corresponding solution was stored as a stock material for the subsequent study described in this paper.

The stock sol 1A was further used for the formulation of a stable "ink" suitable for deposition by piezoelectric inkjet printing. A mixed diluent (MD) was prepared by mixing 25 mL of isopropyl alcohol, 25 mL of propoxyethanol, and 2 mL of ethylene glycol. The stock sol 1A was diluted with variable amounts of the mixed diluent, and a series of printing formulation candidates was prepared and denoted 1B, 1C, 1D, and 1E (see the Results and Discussion section for dilution details). The viscosities, densities, and surface tensions of the resulting formulations were measured by an automatic viscosimeter AVMn (Anton Paar), a density meter DMA4500 (Anton Paar), and a rheometer AR-G2 (TA Instruments), respectively. Preliminary printing tests were performed with all these candidates.

2.3. Optimization of the Ink and Printing Conditions. Jettability and patterning tests were performed with an experimental Fujifilm Dimatix 2831 inkjet printer. The prepared printing formulation candidates were sonicated for 5 min and then loaded into a syringe. A 0.45-μm membrane filter (Pall Corporation, USA) and a blunt needle were attached to the syringe luer port. The printing formulation was filtered and filled into the Dimatix ink tank. A Dimatix 10-pL printing head was attached to the tank and mounted onto the Dimatix printer. At the beginning of the preliminary testing period, the optimal printing conditions were determined: Dimatix Model fluid 2 waveform, 20 V driving voltage, a nozzle temperature of 30 °C, and a substrate temperature of 40 °C. The nozzle span was set to 40 μm (i.e., 25 drops per mm, 625 drops per mm^2). The drop formation characteristics of all the candidates were studied by means of a built-in stroboscopic camera, and the interaction of the printed material with the substrate was observed with an optical microscope. The printing settings were kept constant during the evaluation of the printing performance of all the candidate formulations. The printing performance of all the candidates was evaluated at this stage, and the best performing formulation was selected for the subsequent studies (formulation 1C, see below the Results section).

2.4. Sample Fabrication. The best performing ink formulation was subsequently used for the fabrication of a series of thin hybrid titania-silica film samples of variable thicknesses. Simple square 20 × 20 mm and 40 mm × 40 mm patterns were printed onto the microscopic and custom-cut glass substrates, respectively. Printing was repeated up to four times to obtain different overall thicknesses of titania-silica layers. Each layer was completely dried after printing so that the following layer was printed in the "wet-to-dry" manner. The deposition process was finalized by drying at 110 °C for 30 min to remove the high-boiling point components of the printing composition.

A 1 × 1 cm square patch was printed on one of the FTO strips created by scratching the FTO slides, thus forming the working photoanode, while the second strip remained naked for use as the counter electrode. Photoelectrodes of various thicknesses, with the thickest consisting of ten overprinted layers, were fabricated.

2.5. Sample Analysis. Microphotographs of the printed layers were recorded using a Nikon Eclipse E200 optical microscope equipped with a Nikon D5000 digital camera used with the Nikon Camera Control Pro 2 software. SEM imaging and elemental analysis were performed on a JEOL JSM-7600F scanning electron microscope. The same machine was used for layer thickness estimation by observation of the sample cross sections. The phase composition and crystallinity of the films and powder samples were studied with Panalytical Empyrean and Siemens D5000 X-ray diffractometers. Powder samples were prepared by drying 20 mL of the stock sol 1A and crushing the resulting flakes to fine powder in a quartz mortar.

The film topography was investigated by AFM with a Veeco CP-II instrument operating in the noncontact mode. The probe tip radius was estimated from the minimum feature size to be of approximately 50 nm. The micrographs of different samples were acquired at approximately the same position at the center of the layer, thereby avoiding any possible border effects. At approximately the same position, we scratched the TiO_2 layer with a sharp inox needle. The scratch did not damage the surface of the bottom substrate but enabled the determination of the thickness of the TiO_2 layer. The film topography was characterized by the mean square root of the deviation of the heights from the average height (σ), which is known as the RMS roughness.

The layer thickness was further confirmed by spectroscopic ellipsometric measurements using a Horiba UVISEL spectroscopic ellipsometer in the 200−800 nm range. The optical properties of the printed layers were further characterized by measuring the total transmittance spectra using an Agilent Cary 100 UV−vis spectrophotometer equipped with an integrating sphere. Diffused reflectance spectra were recorded using an Ocean Optics Redtide UV−vis spectrometer, a PX-2 xenon light source and related to a Labsphere Spectralon (r) diffuse reflectance standard. The band gap energy was estimated from Tauc plots[43] based on the Kubelka−Munk function of the reflectance data of bulk powder samples for the XRD analysis.

The hardness of the prepared titania films was studied by the "pencil hardness test" according to the ISO 15184 standard.[44] The pencils used as a measure of the relative hardness exhibit 17 distinct degrees of hardness, ranging from the hardest 9H grade to the softest 9B grade. The hardness of the layer is the same as the hardness of the pencil that does not cause any defect on its surface. Despite being only a relative measure, this method enjoys a general acceptance in the coating industry,[45] and many commercial devices performing this test in manual or semi-automatic ways are available. On the other hand, only smooth surfaces can be measured, and this method is destructive. The scratched coatings were imaged with a Nikon Eclipse E200 optical microscope equipped with a Nikon D5000 digital camera.

Photoelectrochemical characterization was performed at room temperature using a two-electrode setup with the 1 cm^2 titania-silica patch on FTO as the working electrode and the opposite naked FTO strip as the counter electrode. This setup was fitted into a 3 cm light path fluorescence cell, and the measurement was performed with a single source measurement unit. The cell was filled with 0.1 M phosphate buffer (pH = 7) and fitted onto an optical bench equipped with a mercury vapor medium pressure lamp and a narrow bandwidth interference filter centered at 365 nm. The lamp emission was monitored with a Gigahertz Optic X97 Irradiance Meter with a UV-3701 probe, and the irradiance was set to 3 mW/cm^2 by adjusting the aperture of the lamp. Photocurrent measurements were performed with an electrometer driven by the National Instruments LabVIEW platform and by supplying a linear voltage gradient of 10 mV s^{-1} from −0.5 to 2 V. For chronoamperometric measurements under illumination, the applied

DOI: 10.1021/acsami.5b03494
ACS Appl. Mater. Interfaces 2015, 7, 16177−16190

Table 1. Composition and Properties of the Printing Formulations

		surface tension (mN/m)		density (g/cm^3)		viscosity (mPa·s)		
	mixing volumetric ratio of 1A + MD	mean	SD	mean	SD	mean	SD	Z-number
1E	0 + 10	26.23	0.18	0.8556	0.0012	2.1830	0.0059	9.705
1D	1 + 9	27.17	0.18	0.8837	0.0015	3.2444	0.0069	6.754
1C	2 + 8	27.84	0.19	0.9004	0.0016	3.8768	0.0113	5.775
1B	4 + 6	28.60	0.16	0.9372	0.0012	4.7276	0.0097	4.898
1A	10 + 0	32.84	0.13	1.0222	0.0020	5.4214	0.0134	4.779

voltage was set to 1 V, and the lamp radiation was manually chopped at 30 s intervals.

The self-cleaning photocatalytic activity of the different films was demonstrated by a fluorescence test with a solid organic contaminant containing terephthalic acid. The detailed procedure is published elsewhere[46] and describes in full detail all the steps of this sensitive, reliable, and quantitative photocatalytic test consisting of the following steps: (1) preparation of a transparent organic coating (sodium salt of terephthalic acid in cellulose host) over the photocatalyst layer, (2) irradiation of the coating for different times in a photochamber and washing the coating with ethanol/water solution, and (3) analysis of the extracted solution containing oxidized products by high performance liquid chromatography with fluorescence detection (HPLC-FLD).

3. RESULTS AND DISCUSSION

3.1. Optimization of the Ink Formulation and Printing Conditions. The ink surface tension, substrate surface energy, and ink viscosity are the most prominent factors influencing droplet formation and layer merging during the inkjet printing of a functional liquid onto a nonporous nonabsorbing substrate. Apart from these ink properties, the substrate temperature also plays a very important role because it is the main factor influencing the solvent evaporation rate. Lower temperatures result in slow drying, mottling, and dust accumulation, while higher temperatures lead to premature evaporation and banding pattern formation. These general rules also prove to be valid in the case of our hybrid titania-silica sol. The 3-component mixed diluent used for stock sol dilution deliver optimal jetting and drying characteristics. The major components, isopropyl alcohol and propoxyethanol, work as fluid vehicle by carrying suspended titania and silica particles. They differ significantly in their volatility, which contributes to the gradual drying and seamless merging of the printed bands. The minor component, ethylene glycol, acts as humectant that prevents the ink from drying in the printhead nozzles. Table 1 summarizes the dilution ratios and corresponding densities of the printing formulations. Figure 1 depicts the viscosity and surface tension of the tested formulations. Formulation 1C, containing 20 vol % of the stock sol 1A, was identified as optimal for providing a balanced compromise between printing reliability and sufficient dry mass content.

The final surface topologies of the printouts depend on complex interactions between the drop-shaping forces and the surface properties of the substrate used. Several distinctive phases have been identified during drop-spreading on solid nonabsorbing substrates: a kinematic phase, a spreading phase, a relaxation phase, and a wetting phase.[47] The drop dynamics and film formation can be predicted to a certain degree by theoretical descriptors such as the Weber number ($We = \delta \cdot v^2 \cdot d/\sigma$), Ohnesorge number ($Oh = \eta/\sqrt{(d \cdot \sigma \cdot \delta)}$), Z number ($Z = \sqrt{(d \cdot \sigma \cdot \delta)}/\eta$), and Reynolds number ($Re = \delta \cdot v^2 \cdot d/\eta$), where δ is the density, v is the drop velocity, d is the diameter of the nozzle, σ is the surface tension, and η is the viscosity of the liquid. Table 1 also gives the values of the Z number that were used as the

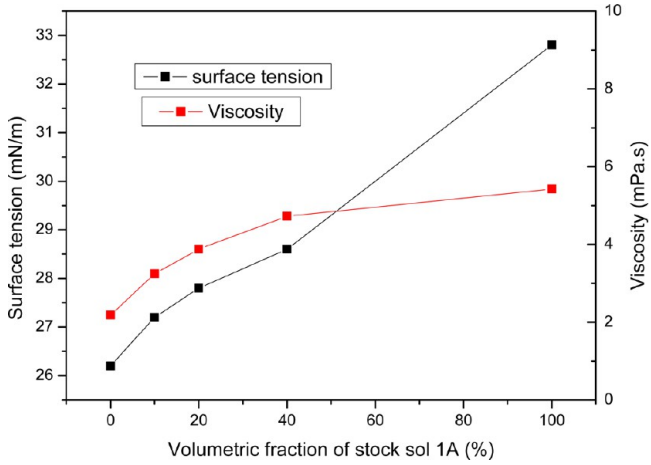

Figure 1. Dependence of the viscosity and surface tension of the tested formulations on the dilution.

indicator of drop formation and printability (e.g., capillary breakoff length and time, droplet volume, and satellite formation). While some theories predict a stable drop formation in drop-on-demand systems when $Z > 2$,[48] others determined that a printable fluid should have a Z value between 1 and 10.[49] It is also known that the lower limit is governed by the viscosity of the fluid and its printing ability, while the upper limit is determined by the point at which multiple drops are formed instead of a single droplet.[50] In our study, the Z values were in the range of 4−9.

The recommended optimal viscosity range for jetting with a Dimatix printer is 10−12 mPa·s, and the recommended optimal surface tension is 28−33 mN/m. Despite the relatively low viscosity of all the studied mixing ratios, their jetting performance was excellent, and a nozzle blockage was only rarely observed. Moreover, printing of the low-viscous formulation did not require viscosity reduction by print head heating, therefore enabling printing at ambient temperature, which was beneficial for the suppression of nozzle drying.

3.2. Layer Surface Morphology. The AFM scans of the TiO_2 layers are presented in Figure 2. The surface morphology in the micrometer range is characterized by the formation of agglomerated grains. The diameter of the observed grains was less than or equal to the radius of the AFM probe tip, which is approximately 50 nm. Comparing the observed diameter of the grains, we note that the diameter did not exhibit a significant dependence on the number of layers, confirming that the average grain diameter did not depend on the number of deposited layers but on the size of the deposited nanoparticles. Because the same nanoparticle composition was used for successive layers, the average diameter did not change. Similar results were obtained from the surface roughness (σ) measurements: σ was calculated from 10 μm × 10 μm area topography scans and ranged between 10 and 16 nm. Generally, σ gradually increased with the number

DOI: 10.1021/acsami.5b03494
ACS Appl. Mater. Interfaces 2015, 7, 16177−16190

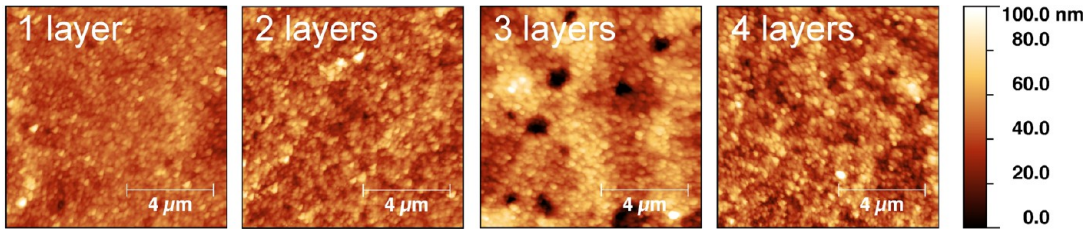

Figure 2. AFM images of the printed samples.

of layers. However, the third layer (Figure 2(c)) presents marginally higher roughness than the fourth layer (Figure 2(d)). This is because the AFM topography imaging was performed after the photoactivity tests. Particularly in the case of the 3-layer films (Figure 2(c)), large voids were observed probably because of film damage. Although these voids were excluded from the σ calculation, the roughness of the surface around these voids was slightly increased, resulting in increased σ. In addition to σ, we also measured the film thickness (see Table 2).

Table 2. Summary of Thickness Data

	AFM		SEM		ellipsometry	
layer	thickness (nm)	RMS (nm)	average thickness (nm)	SD	thickness (nm)	model error (nm)
1	37	10	41	7.9	42	0.4
2	71	11	73	21	72	0.2
3	149	16	115	34	119	0.5
4	161	13	163	10	172	0.3

A more detailed view of the surface texture is provided by SEM (Figure 3). We can resolve the individual grains making up larger flakes. The layer was compact without any obvious regular porosity. A few random grooves or pores seemed to develop in the thicker samples, but the layer was generally even without any major defects or deposition artifacts. The SEM technique was also used to observe layer cross sections (see below).

3.3. Thickness. Thickness is the most important parameter influencing the physicochemical properties of thin layers. Multiple techniques were used to measure and verify the thickness of the printed samples. Because inkjet printing may not necessarily produce even-thickness layers because of the banding phenomenon or clogged nozzles, measuring the samples several times with different methods also provided a means to verify the thickness uniformity.

The SEM cross-section images are depicted in Figure 4. The cut was directed perpendicular to the direction of the printhead movement. In this way, we were able to observe the entire length of the cut and check for printing artifacts and general thickness uniformity. Excellent evenness without any significant variations was observed, indicating the flawless printability of the used formulation and well managed merging of the printed bands. The sample thickness was measured at 10 randomly selected spots along the cut, and the values are reported in Table 2. During the AFM study, the samples of all thicknesses were mechanically scratched, and the resulting edge was analyzed. The accuracy and repeatability of this technique depends on the quality of the scratch. Deformations of soft layers and contamination by peeled material are difficult to avoid and are clearly visible as bright specs in Figure 5. The AFM scans and extracted edge profiles for a single measurement are also reported in Table 2. In addition, the ellipsometric data recorded for the optical characterization were used for the thickness calculation (see the ellipsometric characterization below for details).

The results of all three employed methods are summarized in Table 2 and Figure 6. Because the measurements by the three techniques were performed on different samples, the reasonably good match between the obtained results indicates the good repeatability of both the sample fabrication process and the measurements. The mean thickness of a single layer was approximately 40 nm.

3.4. Mechanical Hardness. The pencil hardness test was performed according to the relevant ISO standard. Figure 7 depicts the optical micrograph for pencils 2B and 3B. We can easily identify the long straight scratches corresponding to entirely removed layers caused by the 2B pencil, while the softer 3B pencil only produced trails of shiny silver graphite flakes on the surface of the analyzed sample. Thus, we can conclude that the thickness of the printed layers is equivalent to that of a 3B pencil.

3.5. Phase Composition. The presence of the anatase phase in the powder sample is manifested by an intense peak at the XRD diffraction angle of $2\theta = 25.4°$, followed by less intense peaks at 38°, 48°, 54°, 62°, etc. (see Figure 8).[51] The peak broadening associated with submicrometer particles is also observed. Quite surprisingly, the peaks at $2\theta = 30.8°$ and 42.4° indicate the presence of brookite. The determination of the brookite content could have been conducted by comparing the peak areas, which, in this particular case, would be difficult to perform unambiguously because of the extensive peak broadening and diffraction maxima overlap. While the formation of brookite at elevated temperatures during the hydrothermal treatment of amorphous titania slurries and organic templates is well documented,[52] its formation at ambient pressure and temperature is less common. Nonetheless, several recent papers confirm our observation and also report brookite formation under similar synthetic conditions.[53,54] The photocatalytic activity of pure brookite is generally inferior to that of anatase but is strongly influenced by its morphology,[55] and mixtures of these two phases can benefit from synergistic effects.[56,57]

3.6. Optical Properties. The total transmission spectra depicted in Figure 9 were referenced to the substrate and therefore reflect the transmission characteristics of the coating only. It is worth noting the perfect transmission in the entire visible region and the absence of interference coloring that is otherwise typical for titania coatings. Figure 10 shows a comparison of the visual appearance of typical samples obtained by sol–gel-calcination (left) and the samples used in this study. Apparently, while the sol–gel-calcination originated samples show strong interference coloring originating in their high refractive index, the reported samples exhibit no visual manifestation of the deposited layer, which makes them well suited for the fabrication of self-cleaning coatings on transparent glass surfaces.

DOI: 10.1021/acsami.5b03494
ACS Appl. Mater. Interfaces 2015, 7, 16177–16190

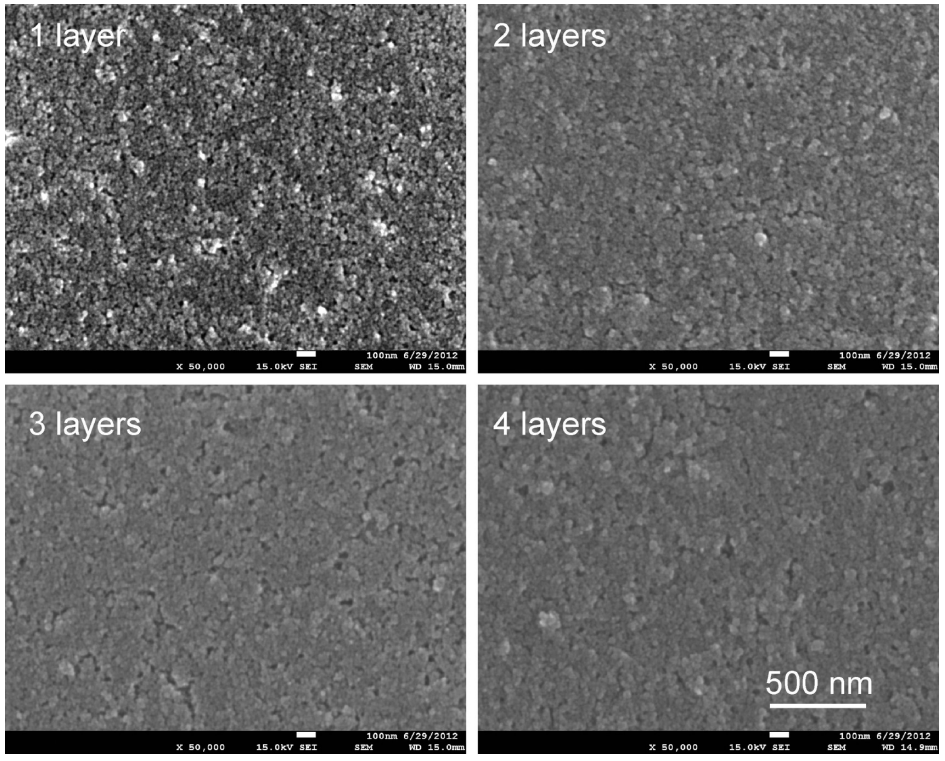

Figure 3. SEM images of the printed samples.

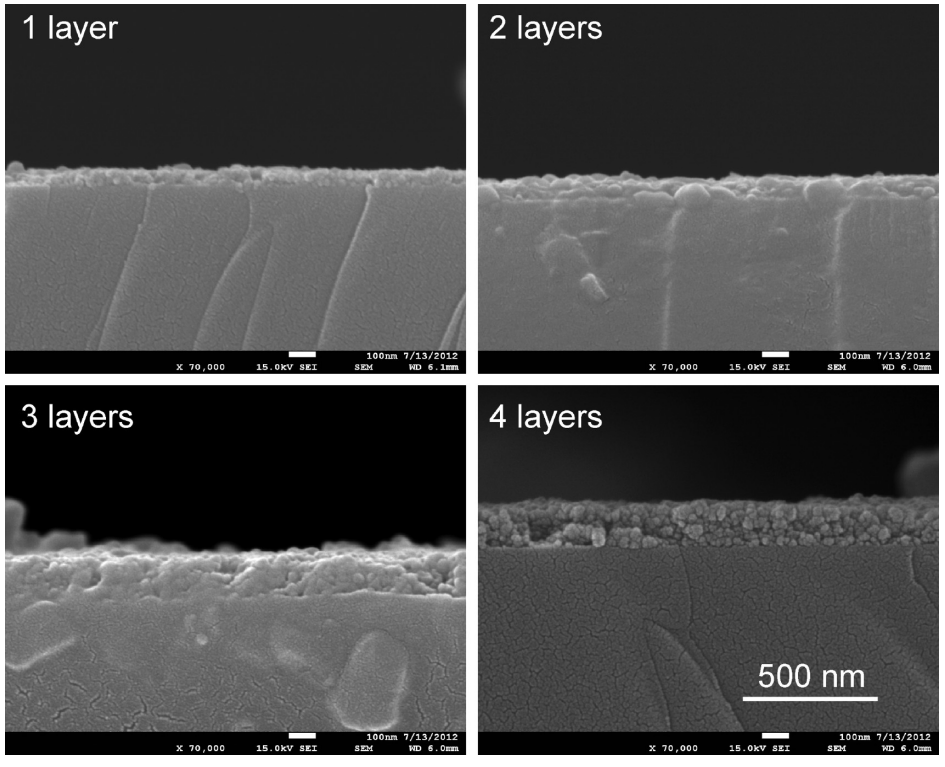

Figure 4. SEM cross section images of the studied samples.

The transmittance plot also indicates that significant absorption occurs below 390 nm. The bandgap was estimated from the Tauc plot depicted in Figure 11. The indirect transition was observed at approximately 3.2 eV, corresponding to 387 nm. The ellipsometric analysis was used for thickness determination and for the determination of the optical constants. The new amorphous ellipsometric model[58] was adopted for both the titania and silica components. The adopted ellipsometric model consists of a mixed titania-silica layer topped by a thin surface roughness layer (see Figure 12). The layer thickness, titania/silica ratio, and model parameters were varied in the fitting procedure. The resulting fitted ellipsometric spectra show

DOI: 10.1021/acsami.5b03494
ACS Appl. Mater. Interfaces 2015, 7, 16177−16190

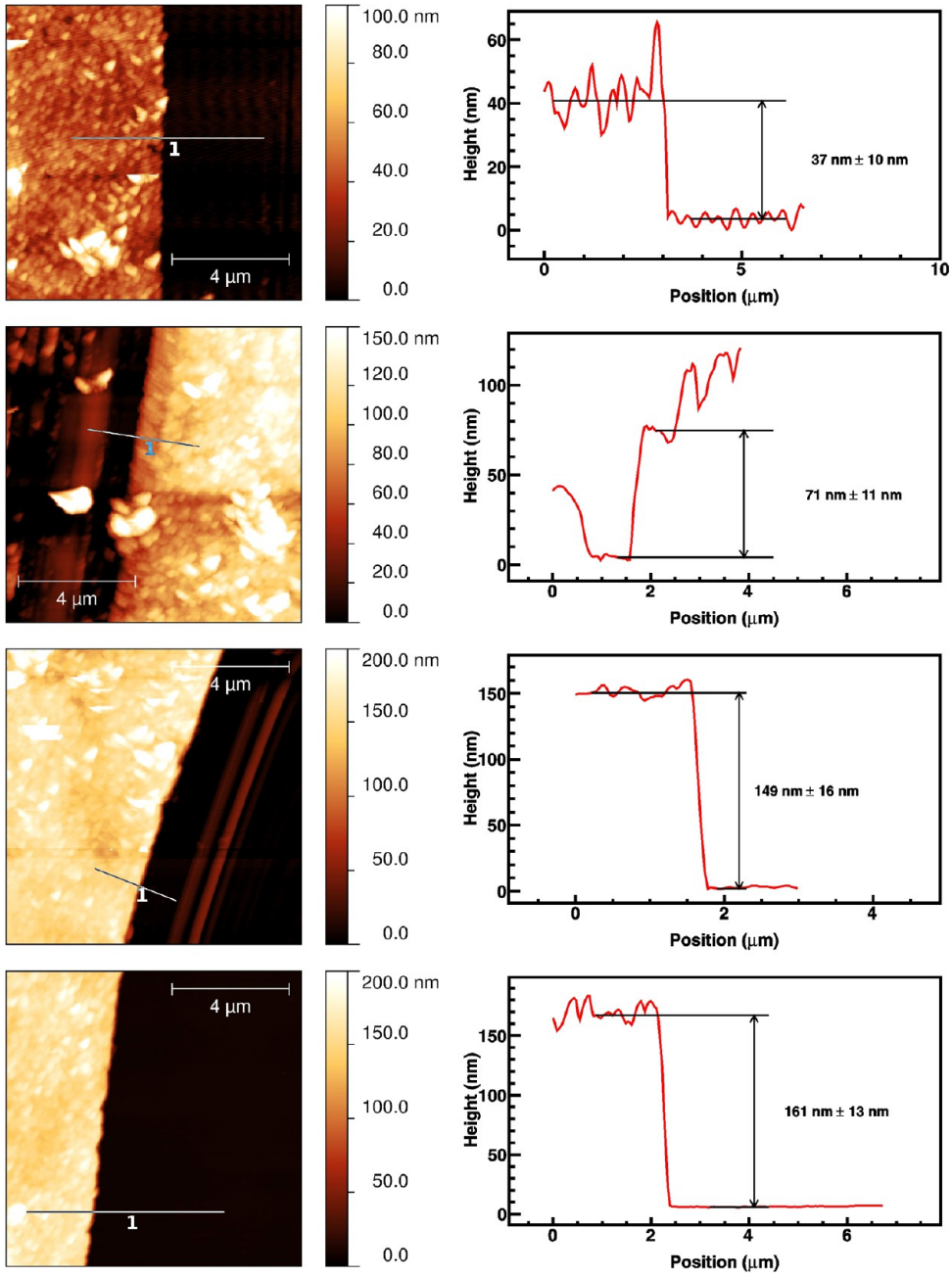

Figure 5. AFM determination of layer thickness.

excellent match with the measured data (χ^2 well below 0.1). While both the thickness and the titania-silica volume ratio values resulting from the fitting procedure were in good agreement with the measured and real values, respectively, the resulting fitted model parameters had to be significantly altered from the default values for bulk materials. The difference can be attributed to the small size and imperfect crystallinity of the titania particles constituting the studied layer.

3.7. Photoelectrochemical Properties. The dependence of the current density on the linearly increasing voltage ramp for the thickest 10-layered sample is illustrated in Figure 13. Because the absorbance of the regular set of 40−160 nm samples was rather low, their photocurrents were also poor. Therefore, thicker photoelectrodes consisting of more overprinted layers were fabricated, and the thickest 10-layered one (ca. 400 nm) finally exhibited an appreciable photocurrent response. The depicted linear voltammogram represents the polarization curves of the studied sample in the dark and under UV irradiation. In the positive potential range, the contribution of the photogenerated current indicates free charge carrier formation and collection, which result from the absorption of UV quanta. The response curve of a typical 100 nm sol−gel originated titania photoelectrode is given for comparison: it features much larger photocurrents and a current plateau[59] in the region of ca. 0.2−1.2 V. Unfortunately, in the case of hybrid titania-silica photoelectrodes, the photocurrent is much lower, and the typical plateau is hardly recognizable.

The chronoamperometric record (Figure 14) illustrates the efficiency, stability, and repeatability of photocurrent generation at a constant potential of 1 V vs the FTO counter electrode. Again, a typical 100 nm sol−gel originated titania photoelectrode response is plotted for comparison. Both depicted samples

DOI: 10.1021/acsami.5b03494
ACS Appl. Mater. Interfaces 2015, 7, 16177−16190

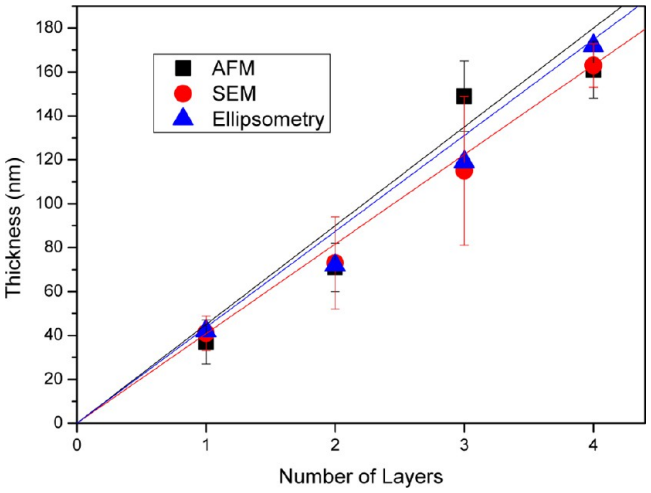

Figure 6. Comparative thickness analysis by different methods.

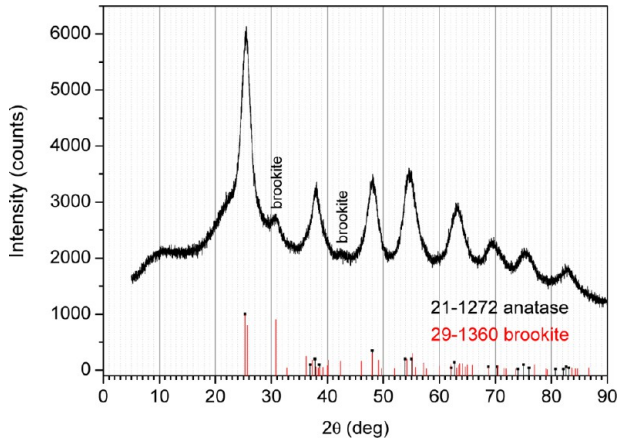

Figure 8. XRD diffraction pattern of the printed titania-silica mixture.

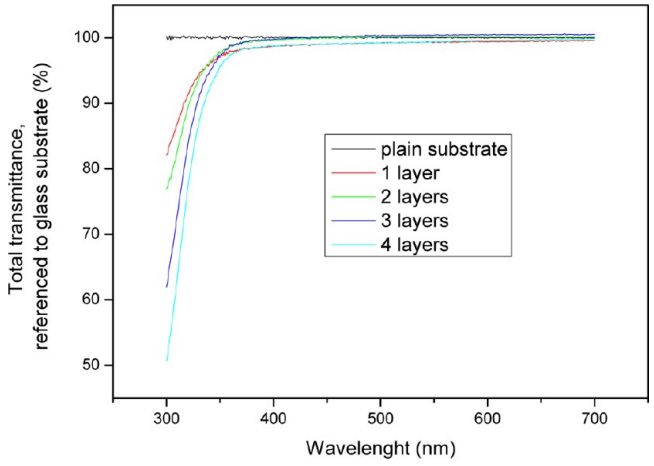

Figure 9. Total transmission UV−vis spectra of the printed layers referenced to the glass substrate.

feature a sharp increase upon irradiation, fast photocurrent equilibrium establishment, and a sharp current decay upon irradiation blocking. However, the photocurrent density of the hybrid 400 nm-thick layer is approximately 10 times smaller than the photocurrent generated in the 100 nm-thick sol−gel-calcination originated titania. Such low photocurrent can be attributed to the limited contact between the titania nanoparticles that are surrounded by the insulating binder and the possibly residual solvent molecules adsorbed on the surface of both the titania and silica nanoparticles. Yet, as shown in Figure 14, the electrodes exhibit essentially no wear or corrosion even after prolonged illumination (10 voltammetric cycles, 40 min).

3.8. Confirmation of Photocatalytic Activity. All four printed layers were tested by a novel, highly sensitive, fluorescence-based method which is based on the deposition of a thin transparent solid layer of terephthalic acid (TPA) over a titania layer. After irradiation of such a system of layers with UV-A light, highly fluorescent hydroxyterephthalic acid (HTPA) − among other degradation products − is formed due to a reaction between the photoexcited TiO_2 and terephthalic acid and can be finally detected by different analytical methods (HPLC-FLD, spectrofluorometer). Figure 15 depicts the kinetic profiles of the HTPA formed during the photocatalytic test conducted with the studied samples. The only difference with respect to the photocatalytic tests described in a published paper[46] was the use of a special plastic holder with 12 or 14 holes (Φ = 9 mm), which was attached to the sample surface using silicon grease. The purpose of such a holder was to separate the parts of the tested photocatalytic layers from one another, creating "wells with a photocatalytic bottom", which allowed us to take a sample from a photocatalytic surface at different times of irradiation for analysis. The samples were obtained by washing

Figure 7. Optical micrographs of the pencil hardness test showing the scratched surface by a 2B pencil (right), while the softer 3B pencil leaves graphite flakes on the surface of the analyzed sample (left).

DOI: 10.1021/acsami.5b03494
ACS Appl. Mater. Interfaces 2015, 7, 16177−16190

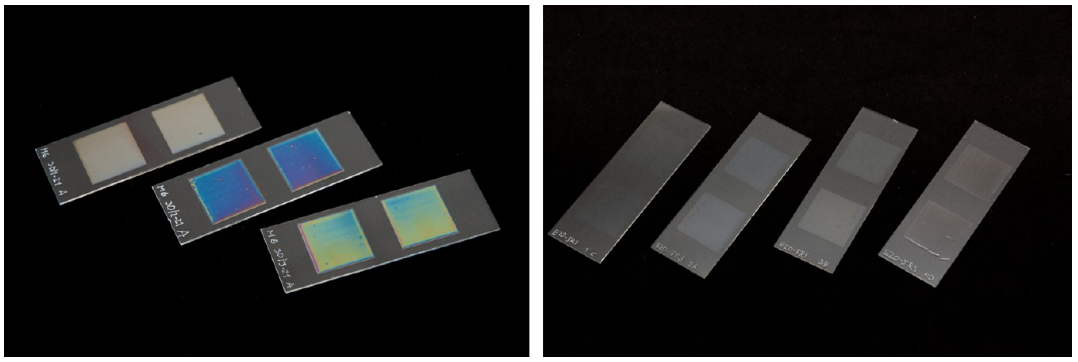

Figure 10. Visual appearance of the titania test patches originating from sol−gel-calcination (left; 1, 2, and 3 layers equivalent to 50, 100, and 150 nm, respectively) and hybrid titania-silica patches (right), both fabricated by inkjet printing.

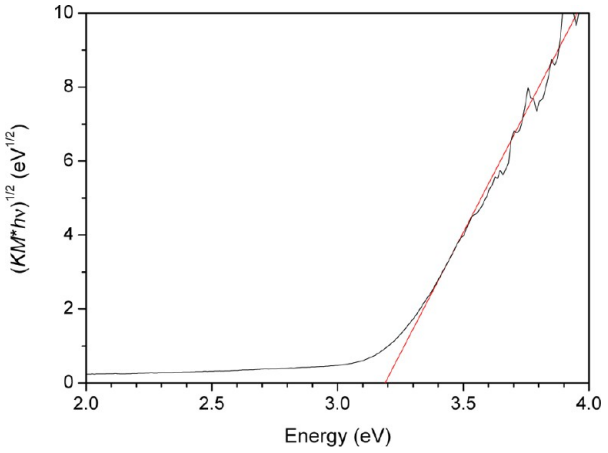

Figure 11. Tauc plot used for bandgap determination. The Kubelka−Munk function (KM) was calculated from the diffuse reflectance spectra of the powders.

the "wells" with an automatic pipet using an ethanol/water mixture. The UV source for the photocatalytic degradation was chosen as suggested in the above-mentioned publication, and the HPLC analyses and fitting of the data according to a simplified kinetic analysis were carried out according to the same publication.[46]

According to our published work, we can conclude that despite the different HTPA and HBA formation rates, the thickness of the photocatalytic layer is in good correlation with the photocatalytic activity of the sample, which is clearly reflected in the increased photocatalytic activity. Table 3 summarizes the HTPA formation rate constants and also provides a comparison with an established commercial self-cleaning glass.

4. APPLICATION PERSPECTIVE

While the benefits and application niches of titania direct pattering have been listed in the introduction, at this point we would like to mention one more specific example illustrating the advantage of the direct patterning approach and the application potential of the reported material: because the charge carrier generation and transport capability of the reported titania-silica hybrid coating are conserved to a certain extent in the hybrid titania-silica layer, we were able to employ it for the fabrication of interdigitated photoelectrochemical cell prototypes intended for water purification.

Recently, the obvious advantage of using an electrical bias in photocatalytic reactions on immobilized semiconductor layers has been demonstrated.[60] The strategy is based on enhancing the electron−hole separation and consequently increasing the quantum yield of the pollutant degradation by the application of an electrical bias, which is possible when the photocatalyst is deposited on an electrically conducting substrate.[61−63] However, in the resulting electrochemical cell, the *iR* drop is one of the factors limiting high-current throughput at moderate bias. If the

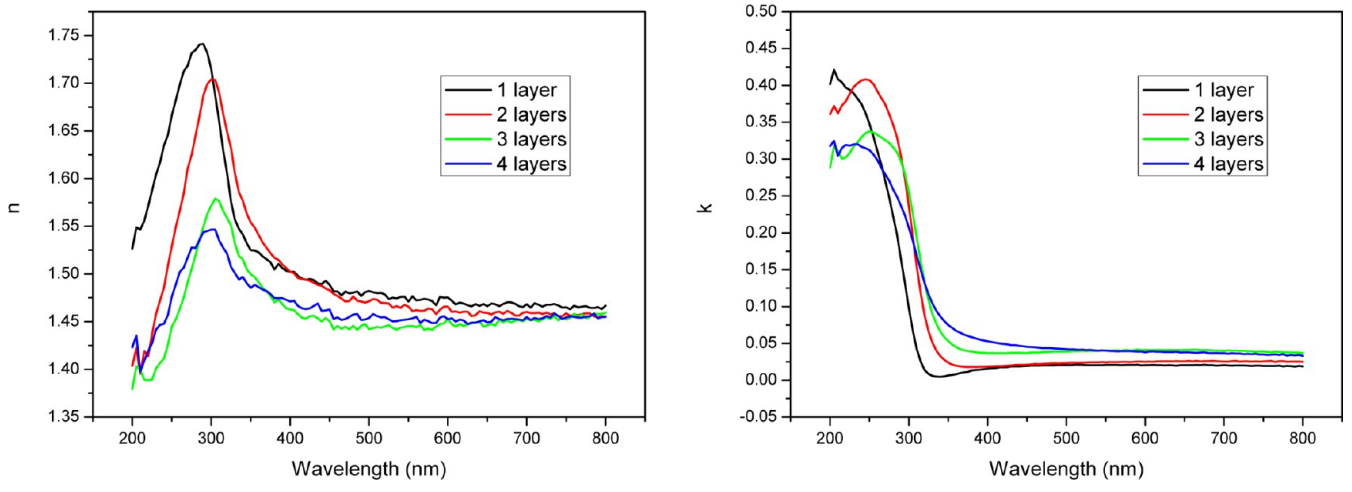

Figure 12. Ellipsometric analysis results−spectral dependencies of the refractive index (left) and extinction coefficient (right). For thickness results, see Table 2 and Figure 6.

DOI: 10.1021/acsami.5b03494
ACS Appl. Mater. Interfaces 2015, 7, 16177−16190

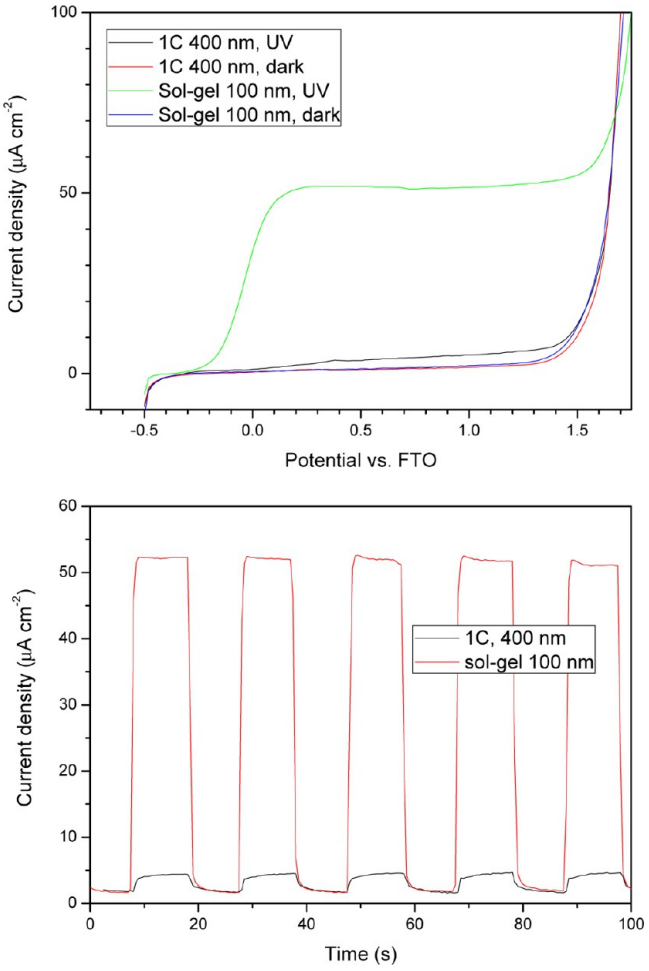

Figure 13. *i*-V curves of titania electrodes fabricated by different methods (top) and chronoamperometric records comparing the currents generated at 1 V bias (bottom).

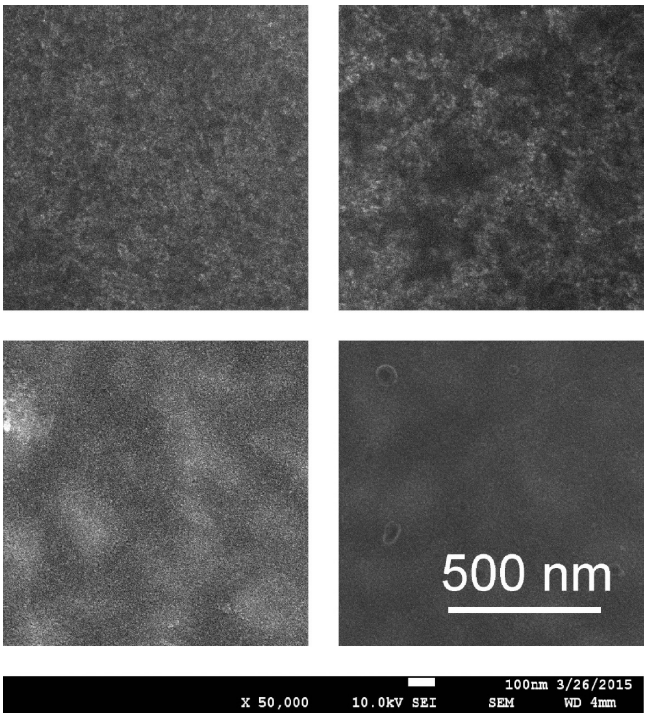

Figure 14. SEM images of the electrode surface. Hybrid titania-silica (top row) and sol–gel (bottom) images before (left column) and after (right) voltammetric experiments. Grains of the substrate FTO layer are apparent in the sol–gel samples.

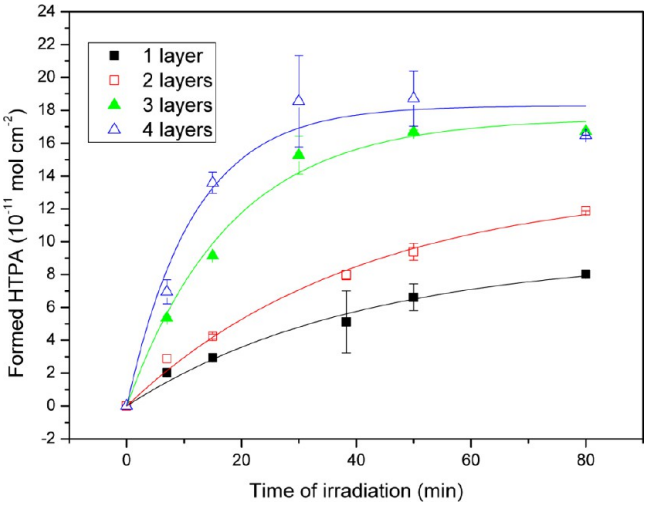

Figure 15. HTPA evolution during UV-A irradiation (moles of HTPA per cm^2).

Table 3. HTPA Formation Rate Constants Depending on the Number of Printed Layers

no. of layers–typical thickness (nm)	HTPA formation rate constant [10^{-9} M/min]
1–40	9.1 ± 1.0
2–80	13.4 ± 1.1
3–120	38.9 ± 3.5
4–160	63.3 ± 10
Pilkington Activ	2.54 ± 0.27

treatment of low ionic strength media (drinking water) is envisaged, means for minimizing the *iR* drop must be secured.

One such means is achieved by using a parallel plate reactor with two opposite electrodes with a small space between them through which the electrolyte is passed.[64] However, the pressure build-up is considerable in a module consisting of many such cells. This drawback can be avoided by using a planar electrochemical cell with two interdigitated electrodes (IDE). The working electrode consists of an electrical conductor covered by semiconducting titanium dioxide. The counter electrode material is not critical as long as sufficient electrical conductivity and corrosion resistance is provided and interdigitated geometry is respected. Such a design ensures two key functions: (1) it suppresses the main obstacle to the efficient use of the absorbed photons, i.e., the recombination of the photogenerated charge carriers, by applying an external electrical bias to the semiconducting photocatalyst and (2) it avoids the reduction of the generated photocurrent due to the *iR* drop, even in electrolytes of low ionic strength. These features make the device an interesting candidate for the photoelectrocatalytic purification of drinking water. The decomposition of model pollutants has been observed on centimeter-scale prototype devices fabricated by standard lithographic techniques using optical copying through contact masks for resist patterning.[65]

The reported hybrid titania-silica formulation may be a potentially useful material for the fabrication of larger devices, which is carried out solely by material printing. Recently, such devices have been fabricated in our lab by a hot process involving

DOI: 10.1021/acsami.5b03494
ACS Appl. Mater. Interfaces 2015, 7, 16177–16190

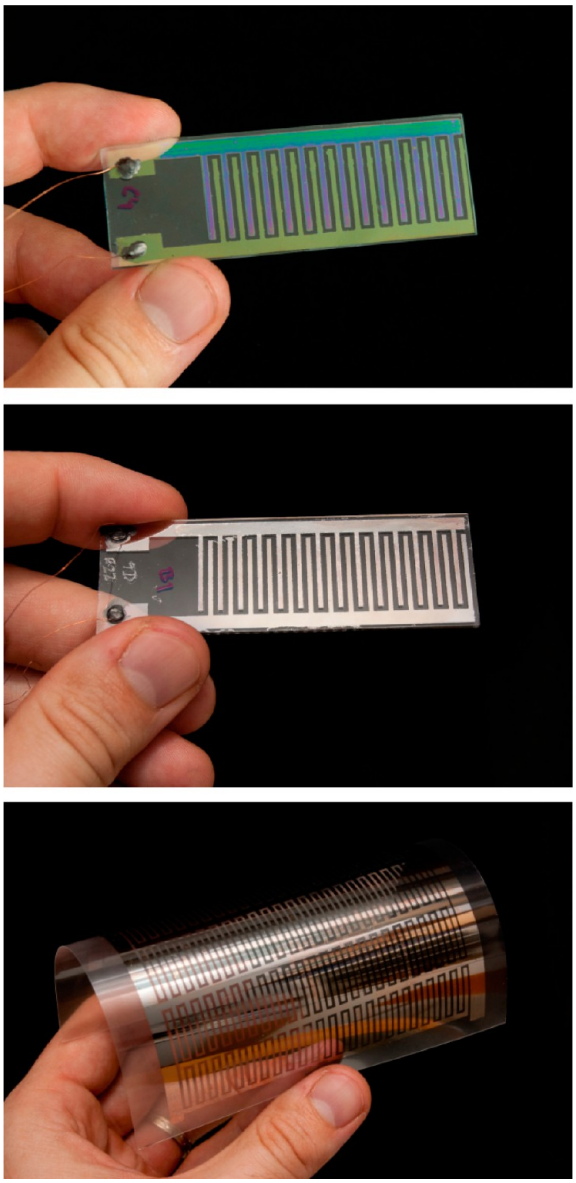

Figure 16. IDE devices fabricated on various substrates: sol−gel-calcination originated titania electrode printed over interdigitated ITO collectors (top), hybrid titania-silica sol printed on top of platinum electrodes (middle), and a prototype 10 × 10 cm IDE device fabricated on a PET substrate (bottom).

the printing of a reverse micelle-based sol−gel[25,66] formulation onto a prepatterned ITO layer and calcining at 450 °C (Figure 16, top). They have been employed for the degradation of model aqueous pollutants, and significant acceleration of the process has been observed.[67] With the reported formulation readily available, we have investigated the option of switching to a cold process, where the active semiconducting layer would be patterned by direct inkjet printing of the reported formulation (Figure 16, middle). Possible further upscaling has been demonstrated by the fabrication of 10 × 10 cm prototypes on PET substrates, which feature interdigitated electrodes fabricated by inkjet printing of nanosilver ink (Figure 16, bottom).

However, as presented in the previous section, the electrochemical properties of the original 1C formulation are rather poor, and the low photocurrent densities do not allow for efficient photoelectrochemical oxidation of pollutants in water. Therefore, two modifications of the deposition process were made to improve its performance:

1) The titania-silica ratio was altered in favor of higher titania content. A new stock sol (2A) containing 75 mol % of titania and 25 mol % of silica was mixed, and a new printing ink (2C) was prepared using the same solvent doses as in the original 1A and 1C formulations. The printability of the 2C ink was equally good, but the reduced binder content resulted into somewhat poorer layer hardness equivalent to 4B on the pencil scale.

2) Various postprinting curing processes were introduced. Thermal sintering of the printed pattern may be one option, inducing not only the complete mineralization of organic compounds but also titania crystallite redistribution and improved contact with the conducting substrate. However, such a process is not compatible with plastic substrates. Photonic annealing may be able to deliver comparable results[68] and ensure compatibility with plastic substrates as the time scale of the process is in the millisecond range, meaning that the required conversion occurs much faster than the thermal damage of the substrate. High-intensity UV-curing was recently reported[69] for photocatalytic coatings of similar composition loaded onto polymeric fibers.

To investigate the possible improvement of the electrochemical properties by these processes, another set of 1 cm^2 electrodes on FTO substrates was printed with the new 2C formulation (10 layers, 400 nm thickness), and various postprinting processing options were selected: one sample was left to dry naturally (marked as the "green body" layer), one was sintered in air at 450 °C for 30 min, one was UV-cured by immersion in a water bath placed 20 cm below an industrial UV−C lamp (model 80 BQL7, 250 W, Ultralight AG, Liechtenstein), and one sample was photonically sintered by exposure to xenon lamp radiation (BP 307, Eurosep Instruments, France). As only a continuously operating lamp was available, photonic annealing was improvised by manually moving the sample into the lamp beam and out in 10 s cycles with 20% duty (2 s irradiation + 8 s dark, 100 cycles total). In this way, the substrate overheating was eliminated, and the sample temperature did not exceed 100 °C. A sol−gel originated electrode acting as a reference was also included in this experiment. Linear sweep voltammetry and amperometry measurements were performed in the same way as with the previous samples.

The photocurrent response curves depicted in Figure 17 indicate that significant but not equal improvement with respect to the performance of the original 1C formulation has been reached for all the tested postprinting processing methods. The sol−gel process originated layers still remained superior in terms of photocurrent generation efficiency, closely followed by the thermally sintered titania-silica layers originating from the 2C formulation. The photonically annealed and UV-cured layers delivered lower photocurrent densities, but a nonetheless acceptable value approaching 20 $\mu A/cm^2$ was achieved with the photonically annealed electrode. The shape of the response curve was similar in all cases, with a well-developed constant current plateau between 0.2 and 1.2 V. As for the amperometry records, all depicted samples featured a sharp current increase upon irradiation, quick photocurrent equilibrium establishment, and a sharp current decay upon irradiation blocking.

Prototype IDE devices of various sizes and finger densities were fabricated on both glass and PET substrates with photonically annealed electrodes, and their oxidizing activity on various model and real pollutants was investigated. Figure 18 depicts the comparison of the short-circuited (electric bias = 0 V between the finger families) and 1 V bias modes of operation of a

DOI: 10.1021/acsami.5b03494
ACS Appl. Mater. Interfaces 2015, 7, 16177−16190

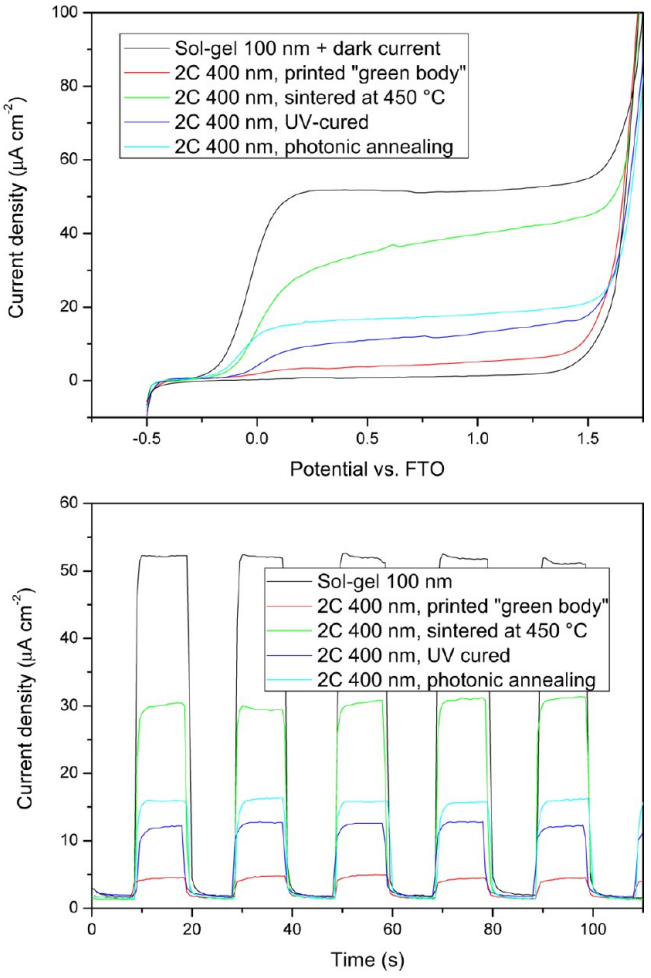

Figure 17. Linear voltammetry (top) and amperometry (bottom) records for various postprinting processing options.

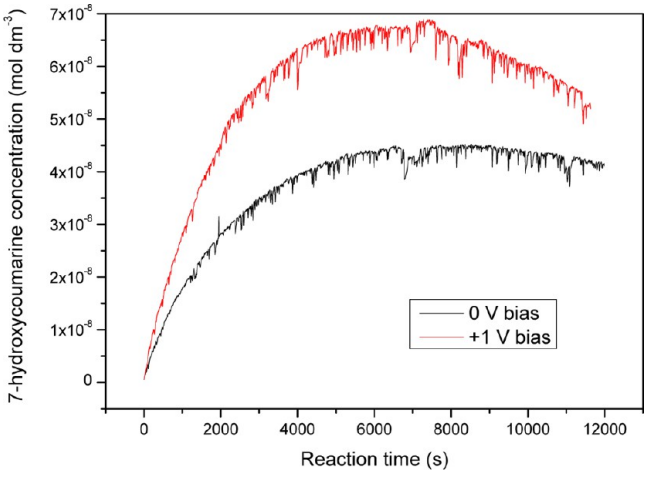

Figure 18. 7-Hydroxycoumarine concentration during the illumination of an IDE device (pairs of 1000 μm wide titania-silica and FTO fingers) immersed in an aqueous solution of coumarin (c_0 = 0.1 mM). The finger families were biased against each other at 0 V or at 1 V.

1000 μm fingered cell (outline as in Figure 16, middle) when a 1×10^{-4} molar solution of coumarin is used as the electrolyte. Coumarin is another very useful fluorescent probe for monitoring the oxidative activity of photocatalysts because one of its oxidation products, 7-hydroxycoumarin, is formed at a constant and repeatable quantum yield and is easily monitored by its strong fluorescence at 460 nm.[70] Figure 18 depicts the changes in 7-hydroxycoumarine concentration (obtained from its fluorescence at 460 nm) during the experiment, forming the typical profile of a reaction intermediate: first, we witness a sharp increase followed by a gradual decrease as 7-hydroxycoumarine is further oxidized. A significant acceleration of the initial rate of 7-hydroxycoumarin formation in the photoelectrocatalytic mode is evident and accounts for suppressed electron−hole recombination in the photoelectrocatalytic experiment at 1 V bias.

5. CONCLUSION

In this paper, we report our contribution to the technology of cold-setting of liquid phase-originated titania coatings. We developed a hybrid titania-silica sol, based on the brick-and-mortar approach, which can be deposited onto a wide variety of surfaces without the need for high-temperature fixing and are suitable for inkjet material printing. The previously patented stock sol containing nanocrystalline titania and amorphous silica particles and with excellent shelf life was used for the formulation of an inkjettable solution. Its printability was theoretically evaluated based on the *Z*-number descriptor and was subsequently confirmed with the research and development level *de facto* standard Fujifilm Dimatix printhead. In this way, well-defined thin hybrid titania-silica patterns of thicknesses ranging from 40 to 160 nm were fabricated by overprinting 1 to 4 layers. Photoelectrodes of up to 400 nm thickness were fabricated by overprinting 10 layers.

Inkjet printing proved to be an elegant method for sol delivery to a substrate. It provides complete control of the deposition process parameters together with an excellent efficiency of precursor use. Moreover, the possibility of precise patterning and the ease of up-scaling make this type of deposition very appealing for the production of sensors, solar cells, etc.

Detailed characterization of the physicochemical properties of the studied samples indicates excellent mechanical and optical properties, making the reported material well suited for the fabrication of transparent self-cleaning coatings on both mineral and organic substrates. The obvious issue of a polymeric substrate resisting to photocatalytic degradation could be easily addressed by the introduction of a pure silica barrier layer. The observed photocatalytic activity is superior to that of commercial CVD-originating products even with the thinnest layer used in this study.

As expected, the photoelectrochemical properties of printed titania nanoparticles were inevitably altered by the introduction of silica in the layer composition. The generated photocurrent density in the hybrid titania-silica samples fabricated with the 1C formulation (1:1 titania to silica molar ratio) was far inferior to the photocurrent response of pure, well-condensed, and crystallized titania electrodes prepared by the sol−gel-calcination process and used as reference.

However, after increasing the titania fraction to 75 mol % and using a postprinting treatment that induced the mineralization of the adsorbed residual solvents and contaminants, the redistribution of titania crystallites, and an improved contact with the conducting substrate, much improvement in the electrochemical properties of printed titania has been achieved. Although thermal sintering remains superior to other postprinting processing methods, photonic annealing and UV−C curing are capable of delivering appreciable photocurrent values and enable deposition on organic substrates. Such processes may be generally useful for

DOI: 10.1021/acsami.5b03494
ACS Appl. Mater. Interfaces 2015, 7, 16177−16190

the preparation of large-area electrodes or interlayers in photonic devices.

Further development of the printed interdigitated electrochemical cells concept was achieved using the reported material. Prototype IDE devices of various sizes and finger densities were fabricated on both glass and PET substrates with the photonically annealed electrodes. Comparative photocatalytic and photoelectrocatalytic experiments with coumarin as the model aqueous contaminant confirmed the functionality of the photoannealed working electrodes based on the beneficial role of an external electrical bias in suppressing photogenerated electron−hole recombination in the semiconducting photocatalyst. The PET-based 10 × 10 cm prototype cell marks the direction for further development: flexible, large-footprint IDE devices will allow the construction of easily replaceable and lightweight IDE cell modules.

AUTHOR INFORMATION

Corresponding Author

*E-mail: petr@dzik.cz.

Notes

The authors declare no competing financial interest.

ACKNOWLEDGMENTS

The authors wish to thank the Ministry of Education, Youth and Sports of the Czech Republic for support by projects *LD14131 Printed Functionalities* and *LO1211 Materials Research Centre at FCH BUT - Sustainability and Development*, with financial support from the *National Program for Sustainability I*.

REFERENCES

(1) Fujishima, A.; Honda, K. Electrochemical Photolysis of Water at a Semiconductor Electrode. *Nature* **1972**, *238*, 37−38.

(2) Chen, X.; Shaohua, S.; Guo, L.; Mao, S. S. Semiconductor-Based Photocatalytic Hydrogen Generation. *Chem. Rev.* **2010**, *110*, 6503−6570.

(3) Pelaez, M.; Nolan, N. T.; Pillai, S. C.; Seery, M. K.; Falaras, P.; Kontos, A. G.; Dunlop, P. S. M.; Hamilton, J. W. J.; Byrne, J. A.; O'Shea, K.; Entezari, M. H.; Dionysiou, D. D. A Review on the Visible Light Active Titanium Dioxide Photocatalysts for Environmental Applications. *Appl. Catal., B* **2012**, *125*, 331−349.

(4) Fujishima, A.; Hashimoto, K.; Watanabe, T. *Tio2 Photocatalysis: Fundamentals and Applications*; Bkc: Tokyo, 1999.

(5) Sobczyk-Guzenda, A.; Pietrzyk, B.; Szymanowski, H.; Gazicki-Lipman, M.; Jakubowski, W. Photocatalytic Activity of Thin Tio2 Films Deposited Using Sol−Gel and Plasma Enhanced Chemical Vapor Deposition Methods. *Ceram. Int.* **2013**, *39*, 2787−2794.

(6) Silva, C. P.; Otero, M.; Esteves, V. Processes for the Elimination of Estrogenic Steroid Hormones from Water: A Review. In *Environmental Pollution*; Elsevier Ltd.: England, 2012; pp 38−58.

(7) Mahmood, M.; Baruah, S.; Anal, A.; Dutta, J. Heterogeneous Photocatalysis for Removal of Microbes from Water. *Environ. Chem. Lett.* **2012**, *10*, 145−151.

(8) Vinu, R.; Madras, G. Environmental Remediation by Photocatalysis. *J. Indian Inst. Sci.* **2010**, *90*, 189−230.

(9) Park, S.; Kim, H. R.; Bang, H.; Fujimori, K.; Kim, B. S.; Kim, S. H.; Kim, I. S. Fabrication and Deodorizing Efficiency of Nanostructured Core-Sheath Tio2 Nanofibers. *J. Appl. Polym. Sci.* **2012**, *125*, 2929−2935.

(10) Wang, C. Y.; Tang, H. J.; Pang, S. H.; Qiu, J. X.; Tao, Y. Enhancing Sunlight Photocatalytic Efficiency of Self-Cleaning Glass by Coating $ZnFeO_4$-TiO_2 Film. *Rare Met. Mater. Eng.* **2008**, *37*, 548−551.

(11) Dunlop, P. S. M.; Sheeran, C. P.; Byrne, J. A.; McMahon, M. A. S.; Boyle, M. A.; McGuigan, K. G. Inactivation of Clinically Relevant Pathogens by Photocatalytic Coatings. *J. Photochem. Photobiol., A* **2010**, *216*, 303−310.

(12) Gan, W. Y.; Lam, S. W.; Chiang, K.; Amal, R.; Zhao, H. J.; Brungs, M. P. Novel Tio2 Thin Film with Non-Uv Activated Superwetting and Antifogging Behaviours. *J. Mater. Chem.* **2007**, *17*, 952−954.

(13) Putz, J.; Aegerter, M. A. Versatile Wet Deposition Techniques for Functional Oxide Coatings on Glass. *Glass Sci. Technol.* **2004**, *77*, 229−238.

(14) Krebs, F. C. Fabrication and Processing of Polymer Solar Cells: A Review of Printing and Coating Techniques. *Sol. Energy Mater. Sol. Cells* **2009**, *93*, 394−412.

(15) Heinzl, J.; Hertz, C. H. Ink-Jet Printing. *Adv. Imaging Electron Phys.* **1985**, *65*, 91−171.

(16) Martin, G. D.; Hoath, S. D.; Hutchings, I. M. *Iop In Inkjet Printing - the Physics of Manipulating Liquid Jets and Drops*; Conference on Engineering in Physics - Synergy for Success, London, England, Oct 05; London, England, 2006.

(17) Tekin, E.; Smith, P. J.; Schubert, U. S. Inkjet Printing as a Deposition and Patterning Tool for Polymers and Inorganic Particles. *Soft Matter* **2008**, *4*, 703−713.

(18) Attia, S. M.; Wang, J.; Wu, G. M.; Shen, J.; Ma, J. H. Review on Sol-Gel Derived Coatings: Process, Techniques and Optical Applications. *J. Mater. Sci. Technol.* **2002**, *18*, 211−218.

(19) Bartkova, H.; Kluson, P.; Bartek, L.; Drobek, M.; Cajthaml, T.; Krysa, J. Photoelectrochemical and Photocatalytic Properties of Titanium (Iv) Oxide Nanoparticulate Layers. *Thin Solid Films* **2007**, *515*, 8455−8460.

(20) Arin, M.; Lommens, P.; Avci, N.; Hopkins, S. C.; De Buysser, K.; Arabatzis, I. M.; Fasaki, I.; Poelman, D.; Van Driessche, I. Inkjet Printing of Photocatalytically Active Tio2 Thin Films from Water Based Precursor Solutions. *J. Eur. Ceram. Soc.* **2011**, *31*, 1067−1074.

(21) Manga, K. K.; Wang, S.; Jaiswal, M.; Bao, Q. L.; Loh, K. P. High-Gain Graphene-Titanium Oxide Photoconductor Made from Inkjet Printable Ionic Solution. *Adv. Mater.* **2010**, *22*, 5265−5270.

(22) Dzik, P.; Vesely, M.; Chomoucka, J. Thin Layers of Photocatalytic Tio2 Prepared by Inkjet Printing of a Solgel Precursor. *J. Adv. Oxid. Technol.* **2010**, *13*, 172−183.

(23) Černá, M.; Veselý, M.; Dzik, P. Physical and Chemical Properties of Titanium Dioxide Printed Layers. *Catal. Today* **2011**, *161*, 97−104.

(24) Morozova, M.; Kluson, P.; Krysa, J.; Zlamal, M.; Solcova, O.; Kment, S.; Steck, T. Role of the Template Molecular Structure on the Photo-Electrochemical Functionality of the Sol-Gel Titania Thin Films. *J. Sol-Gel Sci. Technol.* **2009**, *52*, 398−407.

(25) Morozova, M.; Kluson, P.; Krysa, J.; Dzik, P.; Vesely, M.; Solcova, O. Thin Tio2 Films Prepared by Inkjet Printing of the Reverse Micelles Sol-Gel Composition. *Sens. Actuators, B* **2011**, *160*, 371−378.

(26) Bernacka-Wojcik, I.; Senadeera, R.; Wojcik, P. J.; Silva, L. B.; Doria, G.; Baptista, P.; Aguas, H.; Fortunato, E.; Martins, R. Inkjet Printed and "Doctor Blade" Tio2 Photodetectors for DNA Biosensors. *Biosens. Bioelectron.* **2010**, *25*, 1229−1234.

(27) Yang, M.; Li, L. H.; Zhang, S. Q.; Li, G. Y.; Zhao, H. J. Preparation, Characterisation and Sensing Application of Inkjet-Printed Nanostructured Tio2 Photoanode. *Sens. Actuators, B* **2010**, *147*, 622−628.

(28) Arin, M.; Lommens, P.; Hopkins, S. C.; Pollefeyt, G.; Van der Eycken, J.; Ricart, S.; Granados, X.; Glowacki, B. A.; Van Driessche, I. Deposition of Photocatalytically Active Tio2 Films by Inkjet Printing of Tio2 Nanoparticle Suspensions Obtained from Microwave-Assisted Hydrothermal Synthesis. *Nanotechnology* **2012**, *23*, 165603−165613.

(29) Černá, M.; Veselý, M.; Dzik, P.; Guillard, C.; Puzenat, E.; Lepičová, M. Fabrication, Characterization and Photocatalytic Activity of Tio2 Layers Prepared by Inkjet Printing of Stabilized Nanocrystalline Suspensions. *Appl. Catal., B* **2013**, *138−139*, 84−94.

(30) Oh, Y.; Lee, S. N.; Kim, H. K.; Kim, J. Uv-Assisted Chemical Sintering of Inkjet-Printed Tio2 Photoelectrodes for Low-Temperature Flexible Dye-Sensitized Solar Cells. *J. Electrochem. Soc.* **2012**, *159*, H777−H781.

(31) Shibata, H.; Sakai, H.; Rangsunvigit, P.; Hirano, T.; Abe, M. Preparation and Photocatalytic Activity of Titania Particulate Film with Silica as Binder. *Surf. Coat. Int., Part B* **2003**, *86*, 125−130.

DOI: 10.1021/acsami.5b03494
ACS Appl. Mater. Interfaces 2015, 7, 16177−16190

(32) Chandiran, A. K.; Yella, A.; Stefik, M.; Heiniger, L. P.; Comte, P.; Nazeeruddin, M. K.; Gratzel, M. Low-Temperature Crystalline Titanium Dioxide by Atomic Layer Deposition for Dye-Sensitized Solar Cells. *ACS Appl. Mater. Interfaces* **2013**, *5*, 3487−3493.
(33) Gilmer, D. C.; Gladfelter, W. L.; Colombo, D. G.; Taylor, C. J.; Roberts, J.; Campbell, S. A.; Kim, H. S.; Wilk, G. D.; Gribelyuk, M. A. Low Temperature Chemical Vapor Deposition of Titanium Dioxide Thin Films Using Tetranitratotitanium(Iv). In *Chemical Aspects of Electronic Ceramics Processing*; Kumta, P. N., Hepp, A. F., Beach, D. B., Arkles, B., Sullivan, J. J., Eds.; 1998; pp 45−50.
(34) Uchida, H.; Otsubo, A.; Itatani, K.; Koda, S. Low-Temperature Deposition of Polycrystalline Titanium Oxide Thin Film on Si Substrate Using Supercritical Carbon Dioxide Fluid. *Jpn. J. Appl. Phys., Part 1* **2005**, *44*, 1901−1906.
(35) Weerasinghe, H. C.; Sirimanne, P. M.; Simon, G. P.; Cheng, Y. B. Cold Isostatic Pressing Technique for Producing Highly Efficient Flexible Dye-Sensitised Solar Cells on Plastic Substrates. *Prog. Photovoltaics* **2012**, *20*, 321−332.
(36) Szeifert, J. M.; Fattakhova-Rohlfing, D.; Rathousky, J.; Bein, T. Multilayered High Surface Area "Brick and Mortar" Mesoporous Titania Films as Efficient Anodes in Dye-Sensitized Solar Cells. *Chem. Mater.* **2012**, *24*, 659−663.
(37) Yun, Y. J.; Chung, J. S.; Kim, S.; Hahn, S. H.; Kim, E. J. Low-Temperature Coating of Sol-Gel Anatase Thin Films. *Mater. Lett.* **2004**, *58*, 3703−3706.
(38) Ryu, D. H.; Kim, S. C.; Koo, S. M.; Kim, D. P. Deposition of Titania Nanoparticles on Spherical Silica. *J. Sol-Gel Sci. Technol.* **2003**, *26*, 489−493.
(39) Shen, Y. S. A New Hypothesis of Micro-Region Acid Sites Regarding the Surface Acidity of Binary Oxides. *RSC Adv.* **2012**, *2*, 5957−5960.
(40) Kim, H. J.; Shul, Y. G.; Han, H. S. Photocatalytic Properties of Silica-Supported Tio2. *Top. Catal.* **2005**, *35*, 287−293.
(41) Bao, N.; Wei, Z. T.; Ma, Z. H.; Liu, F.; Yin, G. B. Si-Doped Mesoporous Tio2 Continuous Fibers: Preparation by Centrifugal Spinning and Photocatalytic Properties. *J. Hazard. Mater.* **2010**, *174*, 129−136.
(42) Černigoj, U.; Lavrenčič Štangar, U. Priprava Tio_2/Sio_2 Solov in Njihova Uporaba Za Nanos Samočistilnih in Protizarositvenih Prevlek. 2009.
(43) Tauc, J.; Grigorov, R.; Vancu, A. Optical Properties and Electronic Structure of Amorphous Germanium. *Phys. Status Solidi B* **1966**, *15*, 627−637.
(44) Standardization, I. O. f., Iso 15184: Paints and Varnishes, Determination of Film Hardness by Pencil Test. Geneva, Switzerland, 1998.
(45) Huang, C.; Wu, S. Y.; Tsai, C. Y.; Liu, W. T. The Growth of Organosilicon Film Using a Hexamethyldisilazane/Oxygen Atmospheric Pressure Plasma Jet. *Thin Solid Films* **2013**, *529*, 292−295.
(46) Cernigoj, U.; Kete, M.; Stangar, U. L. Development of a Fluorescence-Based Method for Evaluation of Self-Cleaning Properties of Photocatalytic Layers. *Catal. Today* **2010**, *151*, 46−52.
(47) Rioboo, R.; Marengo, M.; Tropea, C. Time Evolution of Liquid Drop Impact onto Solid, Dry Surfaces. *Exp. Fluids* **2002**, *33*, 112−124.
(48) Fromm, J. E. Numerical-Calculation of the Fluid-Dynamics of Drop-on-Demand Jets. *IBM J. Res. Dev.* **1984**, *28*, 322−333.
(49) Reis, N.; Derby, B. In *Ink Jet Deposition of Ceramic Suspensions: Modelling and Experiments of Droplet Formation*; Symposium on Materials Development for Direct Write Technologies: San Francisco, CA, 2000; pp 65−70.
(50) Jang, D.; Kim, D.; Moon, J. Influence of Fluid Physical Properties on Ink-Jet Printability. *Langmuir* **2009**, *25*, 2629−2635.
(51) Howard, C. J.; Sabine, T. M.; Dickson, F. Structural and Thermal Parameters for Rutile and Anatase. *Acta Crystallogr., Sect. B: Struct. Sci.* **1991**, *47*, 462−468.
(52) Shen, X. J.; Zhang, J. L.; Tian, B. Z.; Anpo, M. Tartaric Acid-Assisted Preparation and Photocatalytic Performance of Titania Nanoparticles with Controllable Phases of Anatase and Brookite. *J. Mater. Sci.* **2012**, *47*, 5743−5751.
(53) Vargeese, A. A.; Muralidharan, K. Effect of Anatase-Brookite Mixed Phase Titanium Dioxide Nanoparticles on the High Temperature Decomposition Kinetics of Ammonium Perchlorate. *Mater. Chem. Phys.* **2013**, *139*, 537−542.
(54) Nikkanen, J. P.; Huttunen-Saarivirta, E.; Zhang, X. X.; Heinonen, S.; Kanerva, T.; Levanen, E.; Mantyla, T. Effect of 2-Propanol and Water Contents on the Crystallization and Particle Size of Titanium Dioxide Synthesized at Low-Temperature. *Ceram. Int.* **2014**, *40*, 4429−4435.
(55) Lopez-Munoz, M. J.; Revilla, A.; Alcalde, G. Brookite Tio2-Based Materials: Synthesis and Photocatalytic Performance in Oxidation of Methyl Orange and as(Iii) in Aqueous Suspensions. *Catal. Today* **2015**, *240*, 138−145.
(56) Gai, L.; Duan, X.; Jiang, H.; Mei, Q.; Zhou, G.; Tian, Y.; Liu, H. One-Pot Synthesis of Nitrogen-Doped Tio2 Nanorods with Anatase/Brookite Structures and Enhanced Photocatalytic Activity. *CrystEngComm* **2012**, *14*, 7662−7671.
(57) Tay, Q.; Liu, X.; Tang, Y.; Jiang, Z.; Sum, T. C.; Chen, Z. Enhanced Photocatalytic Hydrogen Production with Synergistic Two-Phase Anatase/Brookite Tio2 Nanostructures. *J. Phys. Chem. C* **2013**, *117*, 14973−14982.
(58) Forouhi, A. R.; Bloomer, I. Optical Dispersion-Relations for Amorphous-Semiconductors and Amorphous Dielectrics. *Phys. Rev. B: Condens. Matter Mater. Phys.* **1986**, *34*, 7018−7026.
(59) Morozova, M.; Kluson, P.; Krysa, J.; Dzik, P.; Vesely, M.; Solcova, O. Thin Tio 2 Films Prepared by Inkjet Printing of the Reverse Micelles Sol-Gel Composition. *Sens. Actuators, B* **2011**, *160*, 371−378.
(60) Butterfield, I. M.; Christensen, P. A.; Hamnett, A.; Shaw, K. E.; Walker, G. M.; Walker, S. A.; Howarth, C. R. Applied Studies on Immobilized Titanium Dioxide Films as Catalysts for the Photoelectrochemical Detoxification of Water. *J. Appl. Electrochem.* **1997**, *27*, 385−395.
(61) Neumann-Spallart, M. Aspects of Photocatalysis on Semiconductors: Photoelectrocatalysis. *Chimia* **2007**, *61*, 806−809.
(62) Waldner, G.; Bruger, A.; Gaikwad, N. S.; Neumann-Spallart, M. Wo3 Thin Films for Photoelectrochemical Purification of Water. *Chemosphere* **2007**, *67*, 779−784.
(63) Fernandez-Ibanez, P.; Malato, S.; Enea, O. Photoelectrochemical Reactors for the Solar Decontamination of Water. *Catal. Today* **1999**, *54*, 329−339.
(64) Shinde, P. S.; Patil, P. S.; Bhosale, P. N.; Bruger, A.; Nauer, G.; Neumann-Spallart, M.; Bhosale, C. H. Uva and Solar Light Assisted Photoelectrocatalytic Degradation of Ao7 Dye in Water Using Spray Deposited Tio2 Thin Films. *Appl. Catal., B* **2009**, *89*, 288−294.
(65) Neumann-Spallart, M. Photoelectrochemistry on a Planar, Interdigitated Electrochemical Cell. *Electrochim. Acta* **2011**, *56*, 8752−8757.
(66) Dzik, P.; Morozová, M.; Klusoň, P.; Veselý, M. Photocatalytic and Self-Cleaning Properties of Titania Coatings Prepared by Inkjet Direct Patterning of a Reverse Micelles Sol-Gel Composition. *J. Adv. Oxid. Technol.* **2012**, *15*, 89−97.
(67) Dzik, P.; Veselý, M.; Králová, M.; Neumann-Spallart, M. Ink-Jet Printed Planar Electrochemical Cells. *Appl. Catal., B* **2015***17818610.1016/j.apcatb.2014.09.030.
(68) Drahi, E.; Blayac, S.; Borbely, A.; Benaben, P. Impact of Ink Synthesis on Processing of Inkjet-Printed Silicon Nanoparticle Thin Films: A Comparison of Rapid Thermal Annealing and Photonic Sintering. *Thin Solid Films* **2015**, *574*, 169−176.
(69) Gregori, D.; Benchenaa, I.; Chaput, F.; Therias, S.; Gardette, J. L.; Leonard, D.; Guillard, C.; Parola, S. Mechanically Stable and Photocatalytically Active Tio2/Sio2 Hybrid Films on Flexible Organic Substrates. *J. Mater. Chem. A* **2014**, *2*, 20096−20104.
(70) Cernigoj, U.; Stangar, U. L.; Trebse, P.; Sarakha, M. Determination of Catalytic Properties of Tio2 Coatings Using Aqueous Solution of Coumarin: Standardization Efforts. *J. Photochem. Photobiol., A* **2009**, *201*, 142−150.

DOI: 10.1021/acsami.5b03494
ACS Appl. Mater. Interfaces 2015, 7, 16177−16190